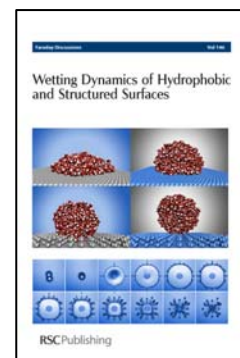


# Faraday Discussions



This paper is published as part of Faraday Discussions volume 146:  
Wetting Dynamics of Hydrophobic and Structured Surfaces

## Introductory Lecture

### [Exploring nanoscale hydrophobic hydration](#)

Peter J. Rosicky, *Faraday Discuss.*, 2010

DOI: [10.1039/c005270c](https://doi.org/10.1039/c005270c)

## Papers

### [Dynamical superhydrophobicity](#)

Mathilde Reyssat, Denis Richard, Christophe Clanet and David Quéré, *Faraday Discuss.*, 2010

DOI: [10.1039/c000410n](https://doi.org/10.1039/c000410n)

### [Superhydrophobic surfaces by hybrid raspberry-like particles](#)

Maria D'Acunzi, Lena Mammen, Maninderjit Singh, Xu Deng, Marcel Roth, Günter K. Auernhammer, Hans-Jürgen Butt and Doris Vollmer, *Faraday Discuss.*, 2010

DOI: [10.1039/b925676h](https://doi.org/10.1039/b925676h)

### [Microscopic shape and contact angle measurement at a superhydrophobic surface](#)

Helmut Rathgen and Frieder Mugele, *Faraday Discuss.*, 2010

DOI: [10.1039/b925956b](https://doi.org/10.1039/b925956b)

### [Transparent superhydrophobic and highly oleophobic coatings](#)

Liangliang Cao and Di Gao, *Faraday Discuss.*, 2010

DOI: [10.1039/c003392h](https://doi.org/10.1039/c003392h)

### [The influence of molecular-scale roughness on the surface spreading of an aqueous nanodrop](#)

Christopher D. Daub, Jihang Wang, Shobhit Kudesia, Dusan Bratko and Alenka Luzar, *Faraday Discuss.*, 2010

DOI: [10.1039/b927061m](https://doi.org/10.1039/b927061m)

## Discussion

### [General discussion](#)

*Faraday Discuss.*, 2010

DOI: [10.1039/c005415c](https://doi.org/10.1039/c005415c)

## Papers

### [Contact angle hysteresis: a different view and a trivial recipe for low hysteresis hydrophobic surfaces](#)

Joseph W. Krumpfer and Thomas J. McCarthy, *Faraday Discuss.*, 2010

DOI: [10.1039/b925045j](https://doi.org/10.1039/b925045j)

### [Amplification of electro-osmotic flows by wall slippage: direct measurements on OTS-surfaces](#)

Marie-Charlotte Audry, Agnès Piednoir, Pierre Joseph and Elisabeth Charlaix, *Faraday Discuss.*, 2010

DOI: [10.1039/b927158a](https://doi.org/10.1039/b927158a)

### [Electrowetting and droplet impalement experiments on superhydrophobic multiscale structures](#)

F. Lapierre, P. Brunet, Y. Coffinier, V. Thomy, R. Blossey and R. Boukherroub, *Faraday Discuss.*, 2010

DOI: [10.1039/b925544c](https://doi.org/10.1039/b925544c)

### [Macroscopically flat and smooth superhydrophobic surfaces: Heating induced wetting transitions up to the Leidenfrost temperature](#)

Guangming Liu and Vincent S. J. Craig, *Faraday Discuss.*, 2010

DOI: [10.1039/b924965f](https://doi.org/10.1039/b924965f)

### [Drop dynamics on hydrophobic and superhydrophobic surfaces](#)

B. M. Mognetti, H. Kusumaatmaja and J. M. Yeomans, *Faraday Discuss.*, 2010

DOI: [10.1039/b926373j](https://doi.org/10.1039/b926373j)

### [Dynamic mean field theory of condensation and evaporation processes for fluids in porous materials: Application to partial drying and drying](#)

J. R. Edison and P. A. Monson, *Faraday Discuss.*, 2010

DOI: [10.1039/b925672e](https://doi.org/10.1039/b925672e)

### [Molecular dynamics simulations of urea–water binary droplets on flat and pillared hydrophobic surfaces](#)

Takahiro Koishi, Kenji Yasuoka, Xiao Cheng Zeng and Shigenori Fujikawa, *Faraday Discuss.*, 2010

DOI: [10.1039/b926919c](https://doi.org/10.1039/b926919c)

## Discussion

---

### [General discussion](#)

*Faraday Discuss.*, 2010

DOI: [10.1039/c005416j](https://doi.org/10.1039/c005416j)

## Papers

---

### [First- and second-order wetting transitions at liquid–vapor interfaces](#)

K. Koga, J. O. Indekeu and B. Widom, *Faraday Discuss.*, 2010

DOI: [10.1039/b925671q](https://doi.org/10.1039/b925671q)

### [Hierarchical surfaces: an \*in situ\* investigation into nano and micro scale wettability](#)

Alex H. F. Wu, K. L. Cho, Irving I. Liaw, Grainne Moran, Nigel Kirby and Robert N. Lamb, *Faraday Discuss.*, 2010

DOI: [10.1039/b927136h](https://doi.org/10.1039/b927136h)

### [An experimental study of interactions between droplets and a nonwetting microfluidic capillary](#)

Geoff R. Willmott, Chiara Neto and Shaun C. Hendy, *Faraday Discuss.*, 2010

DOI: [10.1039/b925588e](https://doi.org/10.1039/b925588e)

### [Hydrophobic interactions in model enclosures from small to large length scales: non-additivity in explicit and implicit solvent models](#)

Lingle Wang, Richard A. Friesner and B. J. Berne, *Faraday Discuss.*, 2010

DOI: [10.1039/b925521b](https://doi.org/10.1039/b925521b)

### [Water reorientation, hydrogen-bond dynamics and 2D-IR spectroscopy next to an extended hydrophobic surface](#)

Guillaume Stirnemann, Peter J. Rossky, James T. Hynes and Damien Laage, *Faraday Discuss.*, 2010

DOI: [10.1039/b925673c](https://doi.org/10.1039/b925673c)

## Discussion

---

### [General discussion](#)

*Faraday Discuss.*, 2010

DOI: [10.1039/c005417h](https://doi.org/10.1039/c005417h)

## Papers

---

### [The search for the hydrophobic force law](#)

Malte U. Hammer, Travers H. Anderson, Aviel Chaimovich, M. Scott Shell and Jacob Israelachvili, *Faraday Discuss.*, 2010

DOI: [10.1039/b926184b](https://doi.org/10.1039/b926184b)

### [The effect of counterions on surfactant-hydrophobized surfaces](#)

Gilad Silbert, Jacob Klein and Susan Perkin, *Faraday Discuss.*, 2010

DOI: [10.1039/b925569a](https://doi.org/10.1039/b925569a)

### [Hydrophobic forces in the wetting films of water formed on xanthate-coated gold surfaces](#)

Lei Pan and Roe-Hoan Yoon, *Faraday Discuss.*, 2010

DOI: [10.1039/b926937a](https://doi.org/10.1039/b926937a)

### [Interfacial thermodynamics of confined water near molecularly rough surfaces](#)

Jeetain Mittal and Gerhard Hummer, *Faraday Discuss.*, 2010

DOI: [10.1039/b925913a](https://doi.org/10.1039/b925913a)

### [Mapping hydrophobicity at the nanoscale: Applications to heterogeneous surfaces and proteins](#)

Hari Acharya, Srivathsan Vembanur, Sumanth N. Jamadagni and Shekhar Garde, *Faraday Discuss.*, 2010

DOI: [10.1039/b927019a](https://doi.org/10.1039/b927019a)

## Discussion

---

### [General discussion](#)

*Faraday Discuss.*, 2010

DOI: [10.1039/c005418f](https://doi.org/10.1039/c005418f)

## Concluding remarks

---

### [Concluding remarks for FD 146: Answers and questions](#)

Frank H. Stillinger, *Faraday Discuss.*, 2010

DOI: [10.1039/c005398h](https://doi.org/10.1039/c005398h)

# Water reorientation, hydrogen-bond dynamics and 2D-IR spectroscopy next to an extended hydrophobic surface

Guillaume Stirnemann,<sup>\*a</sup> Peter J. Rossky,<sup>b</sup> James T. Hynes<sup>ac</sup> and Damien Laage<sup>\*a</sup>

Received 8th December 2009, Accepted 10th February 2010

DOI: 10.1039/b925673c

The dynamics of water next to hydrophobic groups is critical for several fundamental biochemical processes such as protein folding and amyloid fiber aggregation. Some biomolecular systems, like melittin or other membrane-associated proteins, exhibit extended hydrophobic surfaces. Due to the strain these surfaces impose on the hydrogen (H)-bond network, the water molecules shift from the clathrate-like arrangement observed around small solutes to an anticlathrate-like geometry with some dangling OH bonds pointing toward the surface. Here we examine the water reorientation dynamics next to a model hydrophobic surface through molecular dynamics simulations and analytic modeling. We show that the water OH bonds lying next to the hydrophobic surface fall into two subensembles with distinct dynamical reorientation properties. The first is the OH bonds tangent to the surface; these exhibit a behavior similar to the water OHs around small hydrophobic solutes, *i.e.* with a moderate reorientational slowdown explained by an excluded volume effect due to the surface. The second is the dangling OHs pointing toward the surface: these are not engaged in any H-bond, reorient much faster than in the bulk, and exhibit an unusual anisotropy decay which becomes negative for delays of a few picoseconds. The H-bond dynamics, *i.e.* the exchanges between the different configurations, and the resulting anisotropy decays are analyzed within the analytic extended jump model. We also show that a recent spectroscopy technique, two-dimensional time resolved vibrational spectroscopy (2D-IR), can be used to selectively follow the dynamics of dangling OHs, since these are spectrally distinct from H-bonded ones. By computing the first 2D-IR spectra of water next to a hydrophobic surface, we establish a connection between the spectral dynamics and the dynamical properties that we obtain directly from the simulations.

## I. Introduction

While a significant and fruitful effort has been devoted over the past years to the understanding of water thermodynamics next to hydrophobic interfaces and of phenomena such as dewetting,<sup>1,2</sup> a comparable understanding of the water dynamics in these hydrophobic environments has remained elusive. Yet, the dynamics of water next to hydrophobic interfaces is critical for several biochemical processes such as

<sup>a</sup>Dept. of Chemistry, Ecole Normale Supérieure, rue Lhomond, Paris, France. E-mail: guillaume.stirnemann@ens.fr; damien.laage@ens.fr

<sup>b</sup>Dept. of Chemistry and Biochemistry, University of Texas, Austin, TX, USA

<sup>c</sup>Dept. of Chemistry and Biochemistry, University of Colorado, Boulder, CO, USA

protein folding,<sup>1,3</sup> where water expulsion from the hydrophobic core was suggested to be rate-limiting, and amyloid fiber aggregation,<sup>4</sup> which possibly involves protein “smooth spots” with highly labile hydration layers.<sup>5</sup>

Several of us recently characterized the effect of small hydrophobic solutes on the surrounding water dynamics.<sup>6</sup> We showed that the water hydrogen(H)-bond and rotational dynamics are only moderately slowed down by these solutes, due to an excluded volume effect at the H-bond acceptor exchange transition state.

However, this picture cannot be straightforwardly applied to extended hydrophobic surfaces, since the water structural and thermodynamic properties have been evidenced to change dramatically with the curvature of the hydrophobic interface.<sup>1</sup> Next to extended hydrophobic surfaces, water molecules cannot maintain their H-bond network. They reorganize in *anti*-clathrate-like arrangements with water molecule orientations inverted compared to a clathrate hydration structure, where molecules in the first layer sacrifice some of their H-bonds.<sup>7–9</sup> Such changes in the local structure are thus expected to strongly affect the water dynamics.

An improved understanding of water dynamics next to extended hydrophobic surfaces will be first relevant for numerous biomolecular systems such as melittin<sup>10</sup> or other membrane-associated proteins which exhibit large hydrophobic patches. But it will also be of great interest in the context of nanosciences, where water can be conveyed through nanoscopic hydrophobic channels.<sup>11</sup> For these systems, application of macroscopic notions (*e.g.* contact angle, boundary conditions of a fluid flow, friction forces) becomes questionable when only a few thousand of water molecules are involved next to a nano-sized object, *e.g.* a droplet at a flat surface.<sup>2,12</sup> At this scale, the fraction of interfacial waters is extremely important, and the dynamics of individual molecules at the interface can play an important role in the overall dynamics. Molecular studies should therefore provide insights that are not available from macroscopic hydrodynamic approaches.

In this paper, we study an atomically-detailed and uncharged silica surface as a model system. This surface has been shown to be hydrophobic (contact angle of 110°<sup>12</sup>) and has been extensively studied before, mainly from a structural and thermodynamic point of view.<sup>7,13,14</sup> Based on (classical) Molecular Dynamics simulations and analytical modeling, we show how this surface affects water reorientation, and interpret it within the theoretical framework several of us have previously proposed to explain water reorientation in the bulk<sup>15,16</sup> and around small solutes.<sup>6,17–19</sup> We also calculate the two-dimensional infrared (2D IR) vibrational echo spectra, and show that this technique which has recently emerged as a very powerful probe of the H-bond dynamics<sup>20–22</sup> can provide significant new insights about water dynamics at this interface.

The remainder of the paper is organized as follows. We first describe the simulation methodology in section II. We then examine in section III the structure of water molecules at the surface focusing on their orientation, in order to define sub-ensembles of water OHs whose dynamics is discussed in section IV. We then establish a connection with the results that can be obtained from vibrational spectroscopy experiments in section V, before ending with some concluding remarks in section VI.

## II. Methodology

### Simulation details

The model surface has the structure of the (111) face of  $\beta$ -cristobalite, with no silanol group at the surface.<sup>13,14</sup> The surface is rendered hydrophobic by removing all partial charges. The surface atoms thus interact with water only *via* a Lennard-Jones potential, whose parameters were taken from ref. 13. The plate is constituted of 624 atoms distributed over 4 layers of silica, and its resulting size is approximately 3.2 nm  $\times$  3.2 nm  $\times$  0.9 nm. Following previous work,<sup>13</sup> the plate is maintained rigid. The effect

of this approximation on the water dynamics under study is expected to be very limited, since the plate only interacts with the water molecules through a short-ranged, Lennard-Jones interaction, and the amplitude of individual displacements of the plate atoms in a solid would be less than a fraction of an Angström.<sup>13</sup> Water is described by the rigid SPC/E force-field.<sup>23</sup> The simulation box contains the plate, oriented perpendicularly to the  $z$  direction, and 1530 water molecules (for the calculation of 2D-IR spectra, the system is slightly different, as detailed below); the dimensions of the simulation box in the parallel  $x$  and  $y$  directions are larger than the plate size. Our analysis of water dynamics is performed of a restricted region at the center on the plate to avoid finite size effects due to the plate edges.

Molecular Dynamics simulations are performed with the NAMD software.<sup>24</sup> After a first NPT equilibration with Langevin dynamics during 500 ps at  $T = 298$  K and  $P = 1$  bar, a typical trajectory is propagated in the NVE ensemble for 1.5 nanoseconds. The average temperature is  $298 \pm 1$  K. Long-range electrostatic interactions are described by the Ewald-summation and periodic boundary conditions are applied. The distance between two images in the perpendicular  $z$  direction is approximately 3.5 nm; a previous study of the same hydrophobic surface showed that such a separation is sufficient to avoid any confinement effect on water dynamics.<sup>13</sup>

### Spectra

Most experimental 2D IR studies of water dynamics employ an isotopic mixture of dilute HOD in either H<sub>2</sub>O or D<sub>2</sub>O to avoid complications due to intermolecular vibrational energy transfer.<sup>20,21,25</sup> We chose to consider the OD stretch of dilute HOD in H<sub>2</sub>O rather than the OH stretch of HOD:D<sub>2</sub>O because of the greater relevance of H<sub>2</sub>O as a solvent, and of the longer vibrational population lifetime of the OD stretch which allows measurement of experimental spectra at longer delays.<sup>26</sup> The 2D IR vibrational echo spectra were calculated based on the 3rd order nonlinear response functions, including the non-Condon effects and without assuming Gaussian dynamics, following the procedure detailed in ref. 27 and 28. We simulate spectra of dilute HOD in H<sub>2</sub>O from our MD trajectories.<sup>29</sup> The OD stretch vibrational frequency was determined from the local electric field using the frequency map from ref. 27. While in our simulations all waters are H<sub>2</sub>O molecules and not dilute HOD in H<sub>2</sub>O in order to increase the sampling, the effects of this approximation have been verified to be negligible.<sup>28</sup>

### Calculation of jump times

The jump time, or H-bond exchange time, of a water OH from one H-bond acceptor to another is defined as the average time to go from a stable H-bond with the initial acceptor to a stable H-bond with the new acceptor<sup>6,16</sup> (this time will be related to a re-orientation time in Sec. IV.2). Following previous work,<sup>16</sup> the stable H-bond states are defined by tight geometric H-bond conditions ( $R_{OO} < 3.0$  Å,  $R_{OH} < 2.0$  Å,  $\theta_{HOH} < 20^\circ$ ). The jump time  $\tau_{\text{jump}}$  is calculated through the cross time-correlation function between the initial (I) and final (F) states as  $\langle p_I(0)p_F(t) \rangle = 1 - \exp(-t/\tau)$ , where  $p_{I,F}$  is 1 if the system is in state I (F respectively) and 0 otherwise. States I and F are defined within the Stable States Picture<sup>30</sup> to remove the contributions from barrier recrossing<sup>15,16</sup> and absorbing boundary conditions in the product state ensure that the forward rate constant is calculated. Key geometric quantities of these jumps and their amplitude can then be determined from simulations.

## III. Orientation of water molecules next to the surface

The structural arrangement of water molecules next to a hydrophobic surface has been extensively studied before<sup>7,8,10,14,31</sup> on various types of surfaces, including the same surface as the one presently studied.<sup>13</sup> We therefore only summarize the key

features of the water structure that will be used to define the different configurations between which water molecules undergo dynamic exchanges.

The distribution function of water oxygens along the  $z$  direction perpendicular to the plate displays a well-defined first layer of water molecules next to the hydrophobic surface (Fig. 1a). This layer is approximately 3.5 Å-thick, and contains water molecules with different orientations, as revealed by the distance–angle density probability  $P(z, \theta)$  to find a water O–H bond whose oxygen lies at a distance  $z$  from the plate center, and whose axis forms an angle  $\theta$  with respect to a vector normal to the surface, pointing outwards. This probability is then normalized by  $\sin(\theta)$ , removing the bias resulting from the angular variation of the solid angle.<sup>7,32</sup> The probability distribution shown in Fig. 1b. evidences that water molecules within the broad first hydration shell lie along given orientations, leading to separated peaks corresponding to distinct sub-ensembles. These different configurations are schematically represented in Fig. 2.

The first population corresponds to the water OHs pointing toward the surface and lying very close to the surface (Fig. 1b). These OHs, usually referred to as “dangling”, and denoted **D** in the following are not engaged in any H-bond. They result from the strain imposed by the extended hydrophobic surface on the water H-bond network, which is forced to “sacrifice” some H-bonds to accommodate the interface<sup>1</sup> (Note that an H-bond can also be sacrificed by pointing a water lone pair toward the surface,<sup>7</sup> a situation similar in energy to a dangling OH). Such dangling OHs have been evidenced experimentally next to solid surfaces,<sup>9,31,33</sup> water/organic liquid interfaces<sup>33,34</sup> and even very recently around small hydrophobic solutes,<sup>35</sup> mostly by sum-frequency vibrational spectroscopy<sup>9,31,33</sup> which can specifically probe molecules at interfaces. As expected in the absence of any H-bond acceptor, their OH vibration frequency is strongly blue-shifted compared to the average bulk value.<sup>9,31,34,35</sup>

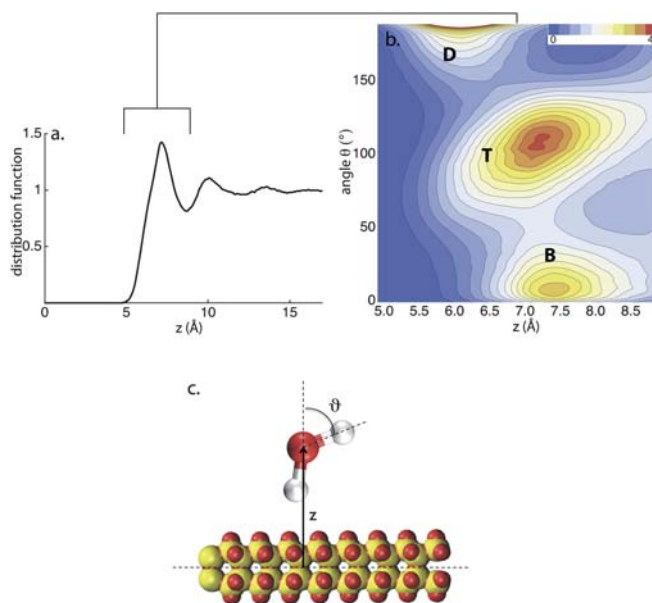


**Fig. 1** (a) Distribution function of water oxygens along the direction perpendicular to the surface, normalized by the bulk density value. (b) Distance–orientation distribution function of water OH bonds as a function of the distance  $z$  and the angle  $\theta$ , normalized by  $\sin(\theta)$ . **D** (dangling), **T** (tangent) and **B** (bulk) refer to the populations of OHs as defined in the main text. (c) Definition of the  $z$  and  $\theta$  coordinates.

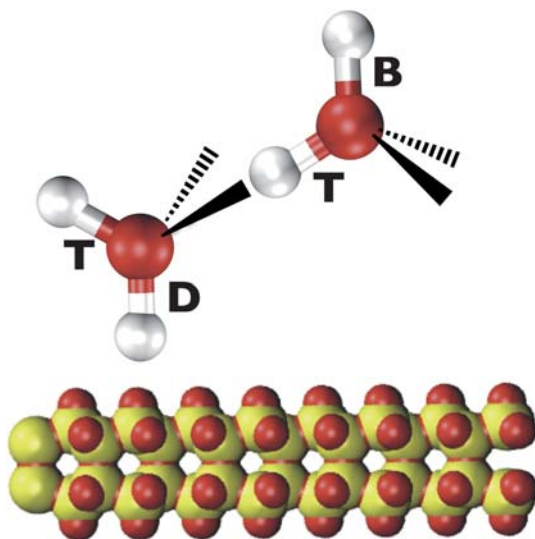


**Fig. 2** Schematic representation of the water structure next to the surface (using different scales for the surface and water molecules). Each oxygen atom is at the center of a tetrahedron formed by its two hydrogen atoms (explicitly represented) and its two lone pairs (black solid and dashed lines). Within the first hydration layer, molecules in direct contact with the surface point one vertex toward the surface, leading to *anti*-clathrate like arrangements (left hand side water on the scheme), with one OH or one lone pair dangling. These molecules are H-bonded to molecules of a second sub-layer, possessing a clathrate-like structure (right hand side). Letters between parentheses indicate to which population each OH belongs.

The second, more broadly spread, OH population corresponds to a configuration tangent (denoted **T**) to the surface (Fig. 2), and represents the major fraction of the first layer total population. These OHs donate an H-bond to other waters within the first layer. The broad peak in the distribution actually results from the contributions of two sub-populations, corresponding to two sub-layers within the first hydration layer. This situation can be analyzed through the local tetrahedral environment surrounding these water molecules. As shown in previous studies,<sup>7</sup> water molecules within the first hydration layer lie in a tetrahedral arrangement resembling that of ice  $I_h$ , although less structured and much more rapidly fluctuating. In an idealized ice structure  $I_h$ , each water tetrahedron can be found in one of two configurations. In the first of those, the tetrahedron can either point its apex to the surface, in an *anti*-clathrate configuration, as for the waters whose other OH is dangling (Fig. 2): the tangent OH then points slightly away from the surface, leading to the shoulder within the broad peak at short distances ( $\sim 7$  Å) and for angles around  $80^\circ$  (this configuration is energetically favored, as the loss of H-bond interactions is limited<sup>7</sup>). In the second of the configurations, the water tetrahedron can lie with one face flat on the surface, in a clathrate-like arrangement (Fig. 2): the tangent OHs then point slightly toward the surface, donating an H-bond to an *anti*-clathrate water, which leads to a contribution to the broad peak at just slightly longer distances from the surface and at angles around  $110^\circ$ . Such clathrate/*anti*-clathrate structures have been observed through MD simulations of water at a broad range of hydrophobic surfaces (realistic surfaces defined at an atomic scale or flat surfaces defined through a single distance dependent repulsive potential; disordered or structured; inorganic or biological<sup>7,10,14</sup>).

Finally, the third population for small angles with the normal vector corresponds to OHs pointing away from the surface, toward the bulk, for water molecules in a clathrate-like configuration. It will be denoted **B** (for bulk) in the following.

Based on the three distinct peaks within the first layer, we define distance and angle criteria to characterize these three sub-ensembles (see Table 1). These different states will be used to determine the rotational dynamics of each population and the exchange kinetics between these states. To eliminate the contribution from transient excursions to the exchange kinetics between states, we use the Stable States Picture<sup>30</sup> to define the three states. This implies that instead of defining only two “transition-state” separatrices between the three populations, each state is defined by boundaries along the distance and angle coordinates close to the corresponding distribution local maximum. A side effect of our definitions is that at any given time, a non-negligible fraction of the total first layer OH population, approximately 55%, does not fall within any of the **D**, **T** or **B** states; however, these systems are short-lived, and very rapidly return to one of the three defined states, on a 0.35 ps timescale. The respective populations in the stable states are 39% in **T**, 3% in **D**, and 3% in **B**, which shows that the vast majority of the OHs next to the hydrophobic surface lie in a tangent configuration.

## IV. Dynamics of water molecules next to the surface

In the following, we examine the reorientational dynamics of the **D**, **T**, and **B** subsets of the first layer OHs we defined in the previous part (see Table 1). The results are interpreted by considering the dynamics of H-bond acceptor exchanges, within and between the different states (see section II for calculation details). An analytic kinetic model describing the exchanges between the different states is then proposed.

### IV.1. Reorientation dynamics

Water reorientation can be followed using the second order Legendre polynomial time-correlation function

$$C_2(t) = \langle P_2[\vec{u}(0) \cdot \vec{u}(t)] \rangle \quad (1)$$

where  $\vec{u}(t)$  designates the orientation of the water OH bond at time  $t$ . It is of particular interest since it can be related to experimental observables in NMR<sup>36</sup> and ultrafast infrared spectroscopy.<sup>37,38</sup> In bulk water at ambient temperature,  $C_2$  decreases mono-exponentially with a 2.5 ps time constant, after a small fast initial drop (<200 fs) due to librations.<sup>39</sup> Bulk simulations based on the SPC/E model<sup>16</sup> lead to an excellent agreement with the experimental data, both from NMR<sup>36</sup> and ultrafast IR<sup>37,38</sup> spectroscopies.

We now compare the reorientation dynamics for OHs according to their initial situation, either in one of the three states **D**, **T**, and **B** within the first shell, or within the second shell, or beyond. We thus consider the  $C_2(t)$  decays for OHs which lie in a given state at time  $t = 0$ , but without imposing any constraint on the future evolution of the system, and thus allowing the system to leave its initial state.

The anisotropy decays starting respectively from the **B** state of the first shell, from the second shell and from the further shells are almost identical (data not shown). They decay mono-exponentially with respective time constants of  $2.7 \pm 0.1$  ps,  $2.8 \pm 0.1$  ps and  $2.6 \pm 0.1$  ps. Since these time scales are the same within error bars,

**Table 1** Definition of the OH populations as defined in the main text, in terms of distances to the surface (0 corresponds to the first non-zero value of the distribution function) and angles with respect to a normal vector pointing outwards (*cf.* Fig. 1)

State	Dangling <b>D</b>	Tangent <b>T</b>	Pointing outwards <b>B</b>	Bulk
Distance to the surface/Å	0–2.7	0–2.7	0–2.7	>3.5
Angle with respect to the normal vector (°)	150–180	70–120	0–20	Any

this illustrates that the influence of the hydrophobic surface on the water dynamics is very short-ranged. The reorientation dynamics starting in the **B** state can therefore be approximated as bulk-like. In the following, **B'** will be used to collectively designate the OHs within the **B** state or within the second layer and further from the surface.

For an OH initially tangent to the surface (**T**), the reorientation is slower than in the bulk, and is non mono-exponential (see inset of Fig. 3 on a logarithmic scale). A single exponential fit on the 2–10 ps interval leads to an effective relaxation time constant of 4.8 ps, thus approximately twice as long as in the bulk. We note that similar retardation factors in the 1.5–2.5 range have been measured by NMR for the water reorientation dynamics at the interface with small hydrophobic peptides<sup>40</sup> or with larger proteins such as BPTI and ubiquitin,<sup>41</sup> whose solvent-exposed surfaces include hydrophobic patches.

For OHs initially dangling (**D**), the  $C_2(t)$  anisotropy decay is dramatically different from the bulk decay and exhibits very unusual features (Fig. 3). The initial drop is very pronounced (more than 50% versus  $\sim 20\%$  in the bulk, *i.e.* anisotropy values of respectively 0.38 and 0.79 after 100 fs, see Fig. 3). This corresponds to very large amplitude librational motions, due to the absence of any surface-fixed H-bond acceptor creating a restoring force; the OH orientation is mainly determined by the three other H-bonds to the water molecule. Following this fast initial decay, the anisotropy decreases on a ps timescale to reach *negative* values, before slowly returning to zero on a much longer time-scale, on the order of a few tens of picoseconds. Such negative anisotropy values are in stark contrast with the bulk behavior where the anisotropy always remains positive.

Several of us recently showed that the reorientation dynamics of water in the bulk<sup>15,16</sup> and around various solutes<sup>17–19</sup> reflects the dynamics of H-bond acceptor exchanges through large angular jumps. We therefore now analyze these acceptor exchanges in each OH population in order to rationalize the observed anomalous orientational relaxations next to the surface.

## IV.2. Hydrogen-bond exchange

In contrast with the traditional rotational diffusion picture, it was recently shown that beyond the initial fast librational decay, water reorientation mainly occurs

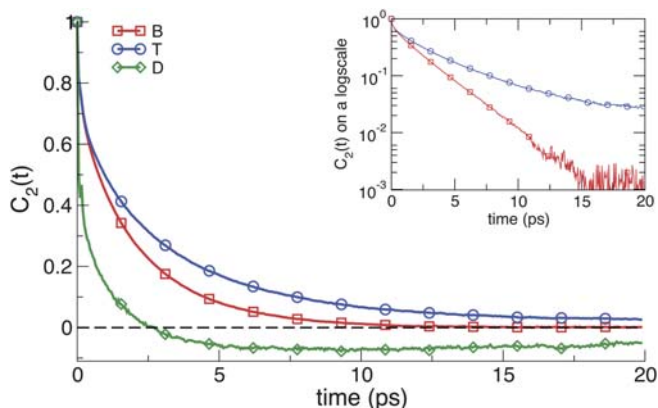


**Fig. 3** Second-order orientational time correlation function  $C_2(t)$  eqn (1). The different curves correspond to distinct initial conditions: OHs initially in the first layer and respectively dangling **D** (green diamonds), tangent **T** (blue circles) or pointing to the bulk **B** (red squares). The decays for OHs initially in the second layer or beyond are superimposed on the **B** decay and are not represented for clarity. The horizontal dashed line corresponds to the vanishing anisotropy value. Inset: **B** and **T** decays on a logarithmic scale; the **D** decay is not represented since it becomes negative.

through large amplitude jumps due to the exchange of H-bond acceptors.<sup>15,16,45,46</sup> It is only once the environment has reorganized to offer a new stable H-bond acceptor that the water OH bond quickly executes a large-amplitude angular jump from its former H-bond partner to this new acceptor.<sup>15,16</sup> The characteristic time of the resulting orientational relaxation was shown to be well described by an analytic molecular jump model, whose two key ingredients are the jump time  $\tau_{\text{jump}}$  (*i.e.* the inverse jump rate constant) and the jump average amplitude  $\Delta\theta$ .

We now use our simulations to characterize and determine  $\tau_{\text{jump}}$  and  $\Delta\theta$  for all the possible jumps occurring next to the interface, for each type of initial and final situations. For this purpose, in addition to the previous geometric conditions defining the stable **D**, **T**, and **B'** states, we add another set of conditions on the H-bond in order to consider only exchanges between stable H-bond states. These correspond to  $R_{\text{OA}} < 3.0$  Å,  $R_{\text{HA}} < 2.0$  Å, and  $\theta_{\text{HOA}} < 20^\circ$ , where A is the H-bond acceptor.

**IV.2.a D state.** We first consider OHs which are initially dangling. These cannot form any stable H-bond since there is no initial H-bond acceptor. However, by extension, the initial stable state is defined here with the same criteria as detailed above, considering as a fictitious acceptor the point on the surface lying at the vertical of the donor oxygen. For an initially dangling OH, the jumps exclusively lead to a tangent **T** situation, as evidenced by the computed jump amplitude distribution (data not shown), which does not contain any noticeable contribution beyond  $130^\circ$  which would have led to a **B** state, and whose average is approximately  $90^\circ$ . This average amplitude is significantly greater than in the bulk<sup>16</sup> ( $\sim 68^\circ$ ), due to the different local water arrangement imposed by the surface. The jump time  $\tau_{\text{jump}}$  is about twice as fast as in the bulk (1.6 ps *vs.* 3.3 ps in the bulk<sup>16</sup>). This acceleration results from the absence of any initial H-bond. Indeed, two of us showed<sup>16</sup> that a significant contribution to the H-bond acceptor exchange activation free energy comes from the free energy cost to elongate the initial H-bond to reach the bifurcated H-bond transition state configuration. Here this contribution vanishes and the jump rate constant accelerates accordingly.

The fast jump from **D** to **T** is also evidenced by the time dependent probability for an initially dangling OH to form an angle  $\theta$  with respect to its initial orientation (Fig. 4a). After a transient initial delay where the average angle rapidly increases, jumps to a tangent situation lead to a distribution centered around an average value of approximately  $90^\circ$ , which very slowly increases with time because of subsequent reorientation once in state **T**. This latter process occurs on a much longer time scale, as shown by the probability distribution for an initially **T** OH (Fig. 4b), and is as discussed below in more detail.

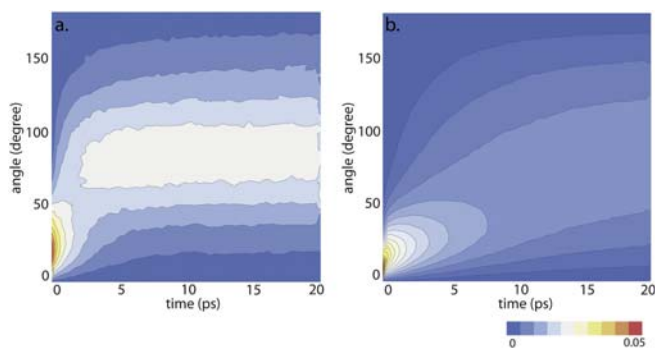


**Fig. 4** Probability density distributions for an OH at time  $t$  to form an angle  $\theta$  with respect to its initial orientation, starting from state **D** (a) or from state **T** (b). For the sake of clarity, only the data after  $t = 0.05$  ps is shown to avoid the initial peaked value of 1 at  $\theta = 0$ .

**IV.2.b T state.** OHs that are initially tangent can jump to form one of three states: (i) either a dangling **D** OH, or (ii) a new H-bond with a water within the first hydration layer, corresponding to a different **T** configuration, or (iii) a new H-bond with a molecule lying in the bulk, leading to a **B'** configuration. The overall jump rate constant (inverse jump time) is the sum of the three rate constants, since these are independent processes.

The **T**  $\rightarrow$  **D** jump corresponds to the reverse reaction with respect to the **D**  $\rightarrow$  **T** jump discussed above. It thus has the same amplitude ( $\sim 90^\circ$ ), but the jump time is much longer (21 ps). The ratio  $\tau_{\text{jump}}^{\text{D} \rightarrow \text{T}}/\tau_{\text{jump}}^{\text{T} \rightarrow \text{D}}$  is indeed equal to the equilibrium constant between the **D** and **T** populations (which is approximately equal to 13) reflecting the large excess of tangent OHs with respect to the dangling OHs.

We now focus on the jump to a new H-bond acceptor, either from the first hydration layer or from further out from the surface. For both cases, the exchange mechanism is the same as in the bulk, as evidenced by the same value of the average jump amplitude ( $68^\circ$ ). As for the kinetics, considering both types of final acceptor together yields a global jump time of 5.9 ps to form a new H-bond. The exchange mechanism is therefore identical to the bulk case, but retarded by a 1.8 factor with respect to the 3.3 ps bulk time.<sup>16</sup>

This retardation phenomenon is completely similar to what we recently evidenced around small hydrophobic solutes,<sup>6</sup> where several of us showed that it stems from an excluded volume effect on the possible transition state locations for the new acceptor. The presence of the hydrophobe (solute or surface) hinders the approach of a new H-bond partner, thus slowing down the exchange rate. The retardation factor  $\rho_V$  is defined as

$$\rho_V = \frac{\tau_{\text{jump}}^{\text{hydrophobic}}}{\tau_{\text{jump}}^{\text{bulk}}} \quad (2)$$

in which  $\tau_{\text{jump}}^{\text{hydrophobic}}$  designates the jump time to a new H-bond partner in the presence of the hydrophobic solute/surface (5.9 ps here). The associated decrease in the transition state (TS) entropy can be estimated in the simulations through the determination of the fraction  $f$  of the transition state locations forbidden by the solute/surface excluded volume.<sup>6</sup> This leads to a transition state excluded volume (TSEV) factor, which provides a quantitative description<sup>6</sup> of the jump time retardation factor  $\rho_V$  through

$$\rho_V = \frac{1}{1-f} \quad (3)$$

Next to convex surfaces (as is the case around small solutes), less than half of the space is forbidden in the TS, and the resulting retardation factor is less than 2; for a wide range of small hydrophobic solutes, the TSEV factor was computed to be approximately 1.4, in good agreement with experimental data.<sup>6</sup>

In the present case of an OH tangent to an extended flat hydrophobic surface, a crude estimate of the excluded volume fraction would be  $f = 1/2$ , leading to a slow-down factor of 2. However, the OH lies slightly above the surface, and the computed TSEV factor is  $\rho_V = 1.8$ , in perfect agreement with the observed retardation on the jump rate given above.

Among the possible new H-bond partners for an initially **T** OH, we now distinguish between the different localizations of final partners. These can first come from the first hydration layer ( $\tau_{\text{jump}} = 9.6$  ps) leading to a final **T** situation where the OH stays tangent to the surface. In this case, the angular jump occurs roughly in a plane parallel to the surface and the rotating OH remains in the first shell. Final partners can alternatively originate from the second shell ( $\tau_{\text{jump}} = 15.2$  ps); the jump arc is therefore perpendicular to the surface and then leads to a final **B'** situation where the OH points away from the surface and interacts with second shell.

It is relevant for the jump times scales that H-bond exchange events induce translational displacements of the water molecules.<sup>17</sup> The slower  $\mathbf{T} \rightarrow \mathbf{B}'$  jumps perpendicular to the surface relative to the faster  $\mathbf{T} \rightarrow \mathbf{T}$  jumps parallel to the surface are consistent with the previous observation of a larger translational diffusion constant for water along a surface than perpendicular to it (see *e.g.*<sup>47</sup> for water next to protein surfaces). As most of the OHs in the first hydration shell are in a tangent  $\mathbf{T}$  state, the above results can also provide a tentative explanation for the well-known decoupling between translational and rotational motions that has been observed next to solutes,<sup>48</sup> hydrophobic surface,<sup>49</sup> and close to the glass transition.<sup>50</sup> The translational dynamics becomes markedly retarded while the rotational dynamics is little affected by the surface (as shown in section IV.1, the  $C_2$  decay for  $\mathbf{T}$  is only retarded by a factor of approximately 2).

**IV.2.c B' state.** Within the  $\mathbf{B}'$  situation, two types of jumps can occur: either a  $\mathbf{B}' \rightarrow \mathbf{T}$  jump, which is the reverse event with respect to the  $\mathbf{T} \rightarrow \mathbf{B}'$  jump described above, or a  $\mathbf{B}' \rightarrow \mathbf{B}'$  jump, which is identical to the jumps characterized in bulk water in previous work ( $\tau_{\text{jump}} = 3.3$  ps and  $\Delta\theta = 68^\circ$ ).<sup>16</sup>

All the jump characteristic times and amplitudes are summarized in the scheme shown in Fig. 5.

**IV.2.d Connection to the orientational relaxation.** The above analysis has shown that the jump rate constants differ between each of the  $\mathbf{D}$ ,  $\mathbf{T}$  and  $\mathbf{B}'$  states. As reorientation mainly occurs through these large angular jumps, this implies that the reorientation times are different within each state. Within the Extended Jump Model (EJM),<sup>15,16</sup> the reorientation time within one state is given by

$$\frac{1}{\tau_{\text{reor}}} = \frac{1}{\tau_{\text{jump}}} \left[ 1 - \frac{1}{5} \frac{\sin(5\Delta\theta/2)}{\sin(\Delta\theta/2)} \right] + \frac{1}{\tau_{\text{frame}}} \quad (4)$$

The different terms are now discussed. It is important to note here that the first contribution, the jump reorientation time, differs from the  $\tau_{\text{jump}}$  jump time by an angular factor<sup>15,16</sup> accounting for the reorientation amplitude each time a jump occurs. In the case of different final partners, as is the case starting from  $\mathbf{T}$ , the overall jump contribution will simply be the sum of each individual jump contribution. An additional minor contribution to the reorientations times arises due to the orientational relaxation of intact H-bonds between jump events, whose time constant is denoted  $\tau_{\text{frame}}$ .<sup>15,16</sup> We now briefly discuss how  $\tau_{\text{frame}}$  is modified for OHs belonging to the one of the three considered states  $\mathbf{D}$ ,  $\mathbf{T}$  or  $\mathbf{B}$ .

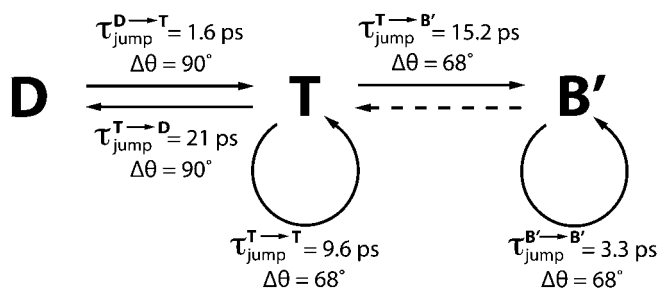


**Fig. 5** Schematic representation of the different H-bond exchanges considered here. Jump times  $\tau$  and jump amplitude  $\Delta\theta$  are given for each type of exchange. When different products are involved, the global rate constant is equal to the sum of the rate constants corresponding to the formation of each product.

Starting from **D**, the  $\tau_{\text{frame}}$  contribution simply vanishes because no H-bond is formed until a jump event occurs. Starting from **T**, the calculated  $\tau_{\text{frame}}$  is 13 ps, twice as long as in the bulk (6 ps<sup>16</sup>) due to the presence of the immobile surface. Finally, for an OH in state **B** (in the first shell but pointing away from the surface),  $\tau_{\text{frame}}$  is the same as in the bulk within error bars (this provides further support for the definition of a single state **B'** including state **B** and the second layer). Surprisingly, the observed retardation of  $\tau_{\text{frame}}$  in both cases is close to the one for the jump time ( $\rho_V$ , eqn (2)); as a consequence,  $\tau_{\text{frame}}$  always remains sufficiently larger than  $\tau_{\text{jump}}$ , such that its contribution to the overall orientational relaxation remains minor.

A further consequence of a jump, which we have not yet elucidated, is the changing of the OH configuration and the induction of transitions between the **D**, **T** and **B'** states. To model the anisotropy decays detailed in section IV.1, we therefore have to determine not only the characteristic reorientation times within each state, but also the exchange kinetics between these states. This is the focus of the following sub-sections.

### IV.3. Kinetic model and interpretation of the anomalous anisotropy decays

We consider the exchanges between the **D**, **T** and **B'** states, where **B'** includes all the first layer OHs pointing to the bulk (**B** state) and all the OHs lying in the second shell and further.

The resulting kinetic scheme is



The rate constants for transitions between the **D** and **T** states, and from **T** to **B'** correspond to the inverse jump times between the corresponding states. A proper description of the exchange from **B'** to **T** would include the effect of translational diffusion within **B'** away from the interface with **T** (see *e.g.* 51). Here we approximate this back reaction by a rate equation, which was shown to yield a satisfactory description at delays shorter than the back reaction inverse rate constant.<sup>52</sup> This rate constant was determined to be  $k_{\text{b}} \approx 1/(45 \text{ ps})$  from the equilibrium constant between the **T** state and the second layer population, which contains all the OHs susceptible to jump to a tangent state.

This simple kinetic scheme (eqn (5)) can then be solved analytically for a given distribution of initial populations, providing the time evolution of each population.<sup>54</sup> Fig. 6 shows the respective populations in each state, starting either from a dangling state **D** (top) or from a tangent state **T** (bottom). These analytic results only require the rate constants determined from the numerical simulations. They can be compared with the direct calculation of the time evolution for the respective populations in the simulations. As shown in Fig. 6, the agreement is extremely good and thus supports this simple kinetic model (the discrepancy for **D** at very short delays corresponds to fast **D**  $\rightarrow$  **T** librational exchanges, not described in our kinetic model).

We now analyze the time-evolutions of the populations for the different initial states to interpret qualitatively the anomalous anisotropy decays shown in Fig. 3.

We first consider the fate of an initially dangling **D** OH (top panel of Fig. 6). The anisotropy decay (Fig. 3) was shown to decay much faster than in the bulk and to reach negative values before slowly returning to an isotropic distribution. This can now be interpreted through the kinetics, which shows that an initial **D** state rapidly jumps within a few ps to a tangent **T** configuration within the first hydration layer. This transiently populated **T** state subsequently decays to populate the **B'** state. Since the average angle between the **D** and **T** configurations is 90°, a crude estimate for the

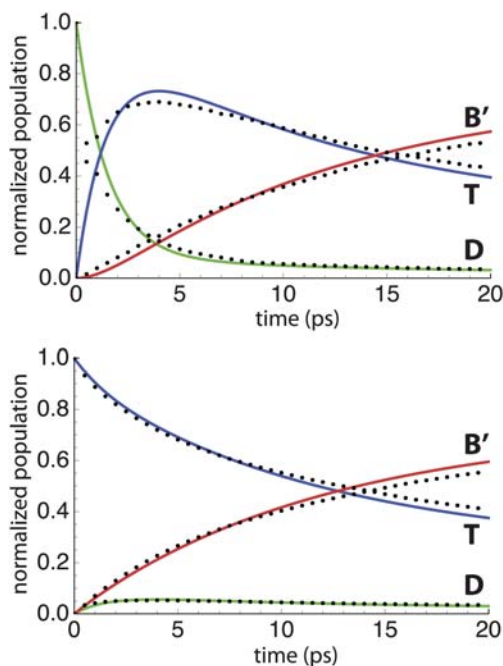


**Fig. 6** Evolution of the normalized population in each state (dangling (green), tangent (red) and bulk (blue)) as a function of time, with different initial conditions: starting from a dangling OH (top panel) or from a tangent OH (bottom panel). Plain lines represents results from our simple kinetic model, and black dots represent the corresponding data, directly extracted from simulations.

$C_2$  anisotropy while in the **T** state is  $P_2[\cos(90^\circ)] = -1/2$ .<sup>55</sup> This explains the negative values (the actual  $C_2$  is less negative than in this simplified picture, mainly because at any given delay, some systems are not in **T** and bring positive contributions to  $C_2$ ); these negatives values are reached on the timescale of the **D**  $\rightarrow$  **T** jump time, *i.e.* 1.6 ps. The slow return of the anisotropy to a vanishing value is due to the **T**  $\rightarrow$  **B'** jumps, whose timescale was shown above to be much slower (15.2 ps).

We now consider the systems which are initially tangent **T** (Fig. 6, bottom panel). For these, the anisotropy decay had been shown (Fig. 3) to decay more slowly than in the bulk, and with a pronounced multi-exponential behavior. This can be explained by examining the time evolution of the populations, which shows that state **T** populates the **B'** state on the same timescale as the reorientation (while state **D** never becomes significantly populated). The anisotropy decay is thus the sum of two contributions. The first one comes from systems which have already switched to the **B'** state and reorient in a bulk-like fashion. The second one originates from systems remaining in state **T**, where the reorientation is slower due to the retarded jump time (slowdown factor of 1.8) and occurs mostly in two dimensions instead of three, due to the dominant contribution of jumps between **T** configurations; the asymptotic anisotropy value is then  $1/4$ <sup>56</sup> and not zero as in the three-dimensional case. The sum of the **B'** and **T** contributions thus leads to an overall anisotropy decay which is slower than in the bulk and not mono-exponential.

## V. Vibrational spectroscopy

We now examine whether the anomalous water dynamics induced by the hydrophobic surface that we have discussed above can be evidenced experimentally.

Most experimental studies of water next to an interface rely on vibrational sum-frequency generation (SFG) spectroscopy, which can specifically probe waters at the interface due to the lack of local symmetry in their environment.<sup>9,31,33,57,58</sup> While this technique yields valuable information about the water structure at the interface, it does not provide any direct information about the dynamics.

Other techniques, although not selectively sensitive to the interface waters, have already been successfully used to investigate water dynamics around solutes. NMR can determine an average water reorientation time within a hydration shell through a concentration-dependence study of the global reorientation time in dilute solutions and the assumption of a two-state bulk/hydration shell model (see *e.g.*<sup>59</sup>). However, in the present case of an interface, it is not clear that such a concentration study could be performed, although measurements of water dynamics around extended hydrophobic systems such as carbon nanotubes have been reported.<sup>60</sup>

Ultrafast infrared spectroscopy can selectively excite the waters within a hydration shell when their vibrational frequency is shifted with respect to the bulk due to the interaction with the solute (see *e.g.* 61,62). As shown experimentally by SFG next to hydrophobic interfaces,<sup>9,31,33,57,58</sup> this is the case for the dangling water OHs whose frequency is blue-shifted. We now examine two types of ultrafast infrared spectroscopy techniques and assess what future studies based on these techniques can reveal about water dynamics next to a hydrophobic interface.

### V.1. Pump–probe spectroscopy

Ultrafast infrared pump–probe spectroscopy can measure the time-resolved anisotropy decay of an initial vibrational excitation, which is proportional to the  $C_2(t)$  orientational time correlation function defined in eqn (1).<sup>37,63</sup> By tuning the frequency of the pump pulse, it is possible to selectively follow the reorientation of waters according to the initial strength of their donated H-bond.<sup>64</sup>

In order to examine the possibilities for this type of spectroscopy, we have calculated the linear infrared spectrum of water next to the hydrophobic surface. As explained in section II, we consider an isotopic mixture of dilute HOD in H<sub>2</sub>O in order to decouple the two water stretching modes and to avoid intermolecular vibrational energy transfer. Fig. 7.a shows the spectrum in the OD stretch frequency region. The dangling ODs lead to a visible peak in the 2700–2750 cm<sup>-1</sup> region. However, this peak overlaps with the broad main peak, whose intensity is much higher. Indeed, some waters from the bulk display very blue-shifted frequencies when they experience a transient H-bond breaking. Even if such events are very brief (< 200 fs<sup>15,22,65</sup>), they are very frequent (more than once per picosecond<sup>53</sup>) and they give a non-negligible contribution to the spectrum on the blue edge. Using a pump frequency in that range will therefore also select these systems in addition to the dangling waters.

Fig. 8 shows the  $C_2(t)$  anisotropy decay calculated for two ranges of initial frequencies, pumping respectively the center of the band (2300–2600 cm<sup>-1</sup>) or the dangling peak region (2700–2750 cm<sup>-1</sup>). The marked initial librational decay for the blue-shifted OHs is due to the large angle of the librational cone in which these systems librate, not only in the **D** state but also in the bulk, where the blue-shifted OH frequency corresponds to a weak H-bond.<sup>39</sup> The subsequent reorientation is faster for systems pumped on the blue edge than in the center of the band, but  $C_2(t)$  does not reach negative values as does the decay from state **D** (see data of Fig. 3 also reported on Fig. 8), due to the large contribution of the bulk OHs. Using pulses linearly polarized along the direction perpendicular to the wall does not sufficiently increase the fraction of dangling OHs in the signal to observe negative anisotropy values. We also note that pumping at the center of the band leads to an anisotropy decay which is intermediate between the ones previously obtained for bulk and tangent OHs, whose initial frequencies are similar. This demonstrates

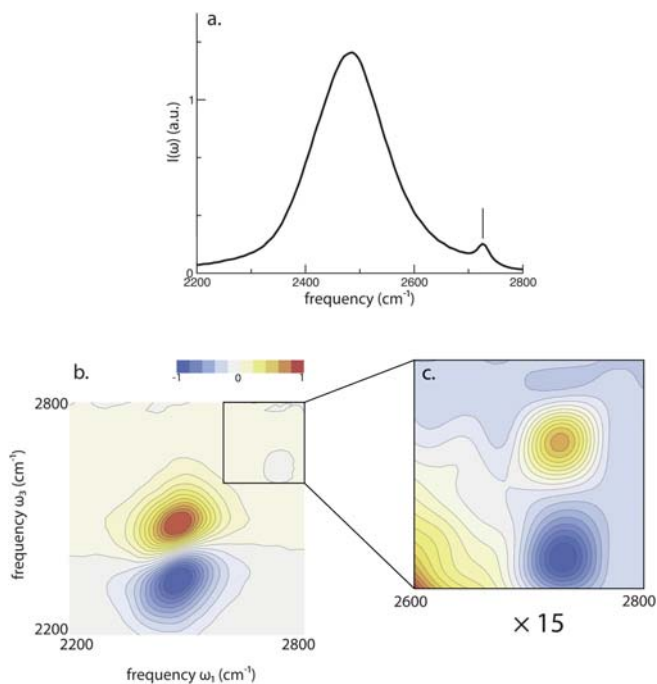


**Fig. 7** (a) Calculated linear spectrum of HOD in  $\text{H}_2\text{O}$  for the system containing the plate and water molecules, polarized along the direction perpendicular to the surface. Bottom: calculated 2D-IR spectra at a delay of  $T = 0.5$  ps, in the whole frequency range (b) and focusing on the peaks corresponding to dangling OHs (c), not visible on the whole spectrum. Each spectrum is normalized with respect to the positive peak height.

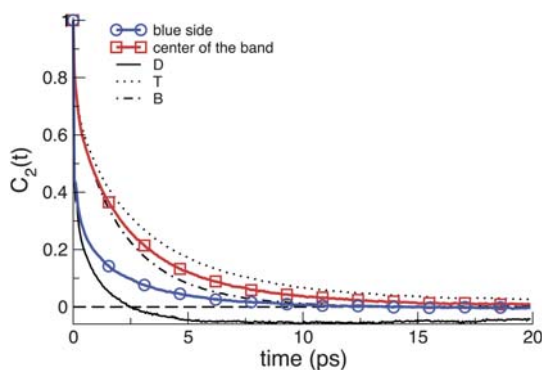


**Fig. 8** Second-order orientational time correlation function  $C_2(t)$  eqn (1), by selecting the initial frequency range. The different curves correspond to distinct initial conditions: initial frequency between  $2300$  and  $2600$   $\text{cm}^{-1}$ , corresponding to the center of the band (red squares); initial frequency between  $2700$  and  $2750$   $\text{cm}^{-1}$ , corresponding to the small peak region (blue circles). Thick black lines (plain, dot-dashed and dashed) represent the anisotropy decay from the geometrically-defined **D**, **T** and **B** states, as in Fig. 3. No particular polarization is used here.

that while pump-probe spectroscopy reveals an anisotropy decay significantly different from that in the bulk, it cannot disentangle the different contributions and selectively follow the dynamics of dangling OHs.

## V.2. Two-dimensional vibrational echo spectroscopy

There is a way to selectively follow the dangling OHs without simultaneously probing the transiently non-H-bonded bulk OHs. This is to take advantage of the much longer lifetime of the dangling state (1.6 ps as shown in section IV.2) with respect to that of the transiently broken H-bonds ( $< 200$  fs<sup>15,22,65</sup>); for transient breakings, the blue-shifted frequency rapidly returns to the center of the band. This can be done *via* two-dimensional infrared (2D-IR) vibrational echo spectroscopy. 2D-IR has recently emerged among ultrafast spectroscopy techniques as a very powerful tool to probe H-bond dynamics.<sup>20,21,25</sup> It measures the time dependence of the water vibrational stretch frequency, which reflects the local environment fluctuations, and has already been successfully applied to study H-bond dynamics in pure water and aqueous salt solutions.<sup>22,26,65–67</sup> 2D-IR spectra can be seen as a correlation map between the excitation frequency  $\omega_1$  and the detection frequency  $\omega_3$  of a given oscillator after a delay  $T$ . It is a Fourier transform technique using broadband excitation pulses, and it is therefore not limited by the time resolution of transient hole burning experiments, due to the required trade-off between time and frequency resolutions.

2D-IR spectra are computed from MD trajectories using the methodology described in Section II. A typical spectrum of HOD in H<sub>2</sub>O is shown in Fig. 7b. It exhibits two main peaks: a positive peak corresponding to the 0–1 OD transition (bleaching), centered around 2450 cm<sup>-1</sup>, *i.e.* the linear spectrum maximum, and a negative peak corresponding to the 1–2 transition (induced absorption). In the following, we will focus only on the positive peaks, even if similar results can be obtained by studying negative peaks, that behave similarly.<sup>62</sup>

An additional diagonal peak on the blue edge reflects the presence of dangling ODs, but it is barely visible on the scale of the main peak. A magnification of the blue region (Fig. 7c) evidences the presence of a system of 0–1 and 1–2 peaks around 2720 cm<sup>-1</sup>. The amplitude of these peaks is very small for two reasons. First, the fraction of dangling ODs is small with respect to the bulk and second, the transition moments are dramatically smaller in the blue region because of non-Condon effects.<sup>27</sup> This last effect is even more pronounced in the 2D spectra than in the linear spectra, because the volume of the peaks is proportional to  $\mu^4$ <sup>62</sup> (compared to  $\mu^2$  for the linear spectra). The relative height of the dangling peak can be increased by a) reducing the distance between the hydrophobic interfaces, thus increasing the fraction of interfacial waters, and b) using pulses linearly polarized along the direction perpendicular to the surface, thus lowering the isotropic contribution of the bulk compared to that of the dangling ODs.

We now discuss the 2D-IR spectral dynamics along the waiting time  $T$ . The time-evolution of both the main peak and the dangling peak results from three effects: spectral diffusion, vibrational population relaxation, and chemical exchange. We now detail each of these different effects.

At short delays ( $< 100$  fs), the frequency memory between excitation and detection is largely preserved, and the 2D correlation spectrum is elongated along the diagonal. In contrast, for longer delays, the frequency diffuses within the spectrum due to the fluctuating forces on the oscillator exerted by the surrounding molecules,<sup>22,66</sup> and the positive-going band in the spectra becomes increasingly symmetrical and round, due to the loss of frequency correlation.

Vibrational population relaxation to the ground state occurs on the vibrational lifetime timescale, *i.e.* 1.45 ps for the OD stretch,<sup>26</sup> and results in an exponential decay of the signal.

The third, chemical exchange, effect appears when the OHs can lie in different states with distinct average frequencies, such as two states with different H-bond strengths.<sup>19,62,68</sup> Systems having undergone an exchange between two states during the waiting time have different excitation and detection frequencies, and lead to off-diagonal cross peaks in the 2D IR spectra. The growth kinetics of these off-diagonal peaks provides the exchange time between the two states.<sup>62</sup> Here, when

an initially dangling (thus blue-shifted) OD jumps to a tangent situation, *i.e.* **D**  $\rightarrow$  **T**, its final frequency falls within the OD spectrum main broad peak. However, the large size of the main peak hides the cross peak, which is not discernable in the spectra.

The exchange kinetics between the **D** and **T** states therefore cannot be measured *via* the appearance of the cross peak, but we will now show it can be determined experimentally from the decay of the diagonal blue-shifted peak, which is shown on Fig. 9 at different delays. We illustrate this approach on our calculated spectra to demonstrate how the exchange time between **D** and **T** can be determined from the 2D IR spectra exclusively, and show that this leads to a timescale very close to that obtained from the direct calculation.

We consider the total volume of the diagonal dangling peak and not its peak height in order to free our approach from spectral diffusion effects.<sup>62</sup> This peak volume is proportional to the population in the vibrationally excited **D** state, and its time evolution with the waiting time *T* is

$$V(T) = \exp[-T(1/\tau_{\text{vib}} + 1/\tau_{\text{jump}}^{\text{D} \rightarrow \text{T}})] \quad (6)$$

where  $\tau_{\text{vib}}$  designates the vibrational lifetime and  $\tau_{\text{jump}}^{\text{D} \rightarrow \text{T}}$  is the **D**  $\rightarrow$  **T** jump time. In our calculated 2D spectra, we employ the same  $\tau_{\text{vib}}$  value (1.45 ps) for all the ODs, even though vibrational lifetimes at interfaces can be different from the bulk.<sup>69</sup> However, note that such vibrational lifetimes can be experimentally measured through a separate set of pump-probe experiments,<sup>62</sup> or they can be calculated<sup>70</sup> but such calculations are beyond the scope of the present study. Therefore, the decay of the peak volume due to vibrational lifetime can be experimentally determined (although we fix it to the bulk value here) and once it is known, an exponential fit of the peak volume decay provides the jump time. Fig. 9 shows the evolution of the blue diagonal peak with time.

The time decay of the blue diagonal peak volume determined from our calculated spectra is shown in Fig. 10. It exhibits an initial (< 200 fs) fast drop of the peak volume, which is due to the blue-shifted OHs from the bulk whose frequency very rapidly returns to the center of the band.<sup>65</sup> Beyond this initial decay, only the **D** OHs remain, and the decay is monoexponential. Using eqn (6) and the vibrational lifetime, a decay time of  $1.9 \pm 0.2$  ps is determined, in good agreement with the 1.6 ps value from the direct determination detailed in section IV.2. We have checked that this time is only weakly sensitive to the definition of the blue peak boundaries.

This clearly demonstrates that 2D-IR will provide experimental information on H-bond dynamics next to a surface that until now have been only accessible through simulations. Current developments in SFG-2D-IR<sup>71</sup> also appear extremely promising in combining the surface-sensitivity of SFG with the time-correlation information provided by the 2D-IR approach.

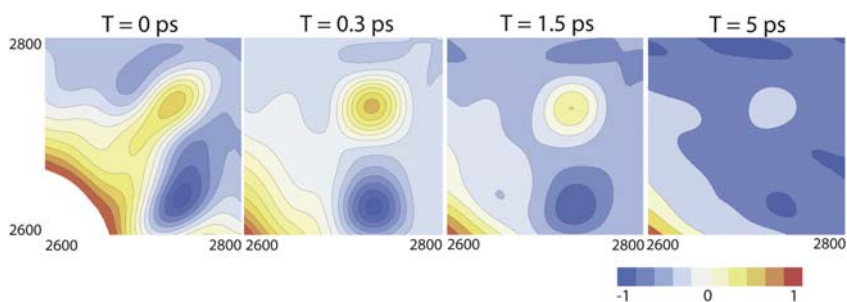


**Fig. 9** 2D-IR spectra in the region of dangling OHs at several delays. The horizontal and vertical axes correspond respectively to the excitation and detection frequencies. To evidence the peak decay due to exchange, each spectrum is normalized by a factor  $e^{-T/1.45\text{ps}}$  corresponding to the global decay of the spectra because of vibrational population relaxation.

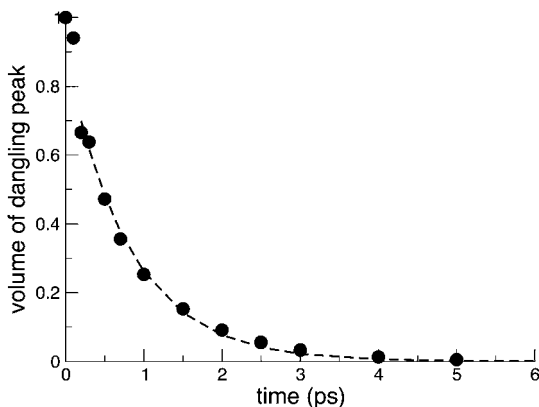


**Fig. 10** Evolution of the dangling peak volume as a function of time, normalized with respect to its initial value (filled circles). The dashed line represents the fit of these points after 200 fs, allowing determination of the jump time.

## VI. Concluding remarks

Based on simulations and analytic modeling, we have presented an extensive study of water dynamics next to a hydrophobic surface. While previous studies have mostly considered the dependence of the water dynamics on the distance from the water oxygen to the surface,<sup>7,14,49</sup> we have shown that considering the orientation of water OHs allows a more effective rationalization of the behavior. Indeed, depending on its orientation, a water OH experiences different environments, which play a critical role in its dynamics.

Most OHs in the first hydration layer are tangent to the surface. We showed that their reorientational dynamics is retarded by a factor close to 2 with respect to the bulk. We quantitatively explained this slowdown, within the Extended Jump Model, by a transition state excluded volume effect on the H-bond exchange mechanism, the presence of the surface hindering the approach of a new H-bond partner. The effect is very similar to the case of small hydrophobic solutes,<sup>6</sup> but is more pronounced because of the larger excluded volume induced by the extended surface.

Some other OHs within the first layer lie in a dangling configuration pointing to the hydrophobic surface, due to the sacrifice of some H-bonds imposed by the surface. They reorient much faster than bulk OHs. The second order orientational correlation function for these dangling OHs takes negative values during its decay, which were shown to be due to an exchange with the more stable tangent configuration.

Finally, we demonstrated that the exchange timescale between dangling and tangent configurations can be measured by 2D-IR experiments, which can selectively follow the spectrally distinct dangling OH population. We trust that future experiments will be able to confirm the very fast dynamics of a sub-ensemble of OHs next to the hydrophobic surface.

The present analysis should find numerous extensions. First, this framework could be applied to the water/organic liquid interface.<sup>72</sup> This liquid interface is expected to be similar to the present solid interface; the organic liquid is also hydrophobic and capillary waves have little influence on the water dynamics.<sup>72</sup> Recent simulation studies on such interfaces<sup>72,73</sup> have shown that water reorientation is strongly anisotropic next to the interface and depends on the initial OH orientation, and, further, that on average the H-bond exchanges within the first layer are slowed down by a factor of 1.4 with respect to the bulk and occur through larger amplitude jumps (84°). Such conclusions are completely consistent with our description here. Relative considerations should prove useful for the water–air interface.

The perspective of our present work can also be extended to surfaces with an increasing hydrophilic character, in connection with a recent simulation study that has evidenced that next to a surface gradually changed from hydrophobic to hydrophilic,<sup>49</sup> the average water reorientation time within the first layer exhibits a non-monotonic character. This time is first retarded by a factor of approximately 2 with respect to the bulk for the most hydrophobic case; it then first decreases with increasing hydrophilicity to nearly reach the bulk reorientation time, before increasing again for even more hydrophilic surfaces to eventually reach a value retarded by a factor of approximately 3 with respect to the bulk.<sup>49</sup> While this behavior was explained through transient ice-like structures,<sup>49</sup> our present work can offer an alternative explanation which emphasizes consideration of the total H-bond environment in analyzing the water dynamics; this would be the aim of future investigations.

## VII. Acknowledgments

This work was supported in part by NSF grants CHE-0750477 (JTH) and CHE-0910615 (PJR).

## References

- 1 D. Chandler, *Nature*, 2005, **437**, 640–647.
- 2 B. J. Berne, J. D. Weeks and R. Zhou, *Annu. Rev. Phys. Chem.*, 2009, **60**, 85–103.
- 3 T. Kimura, A. Maeda, S. Nishiguchi, K. Ishimori, I. Morishima, T. Konno, Y. Goto and S. Takahashi, *Proc. Natl. Acad. Sci. U. S. A.*, 2008, **105**, 13391–13396.
- 4 A. Fernandez and R. S. Berry, *Proc. Natl. Acad. Sci. U. S. A.*, 2003, **100**, 2391–2396.
- 5 A. De Simone, G. G. Dodson, C. S. Verma, A. Zagari and F. Fraternali, *Proc. Natl. Acad. Sci. U. S. A.*, 2005, **102**, 7535–7540.
- 6 D. Laage, G. Stirnemann and J. T. Hynes, *J. Phys. Chem. B*, 2009, **113**, 2428–2435.
- 7 C. Y. Lee, J. A. McCammon and P. J. Rossky, *J. Chem. Phys.*, 1984, **80**, 4448–4455.
- 8 M. C. Gordillo and J. Marti, *Phys. Rev. B: Condens. Matter Mater. Phys.*, 2008, **78**, 075432.
- 9 Y. R. Shen and V. Ostroverkhov, *Chem. Rev.*, 2006, **106**, 1140–1154.
- 10 Y. K. Cheng and P. J. Rossky, *Nature*, 1998, **392**, 696–699.
- 11 J. C. Rasaiah, S. Garde and G. Hummer, *Annu. Rev. Phys. Chem.*, 2008, **59**, 713–740.
- 12 N. Giovambattista, P. G. Debenedetti and P. J. Rossky, *J. Phys. Chem. C*, 2007, **111**, 1323–1332.
- 13 N. Giovambattista, P. J. Rossky and P. G. Debenedetti, *Phys. Rev. E: Stat., Nonlinear, Soft Matter Phys.*, 2006, **73**, 041604.
- 14 S. H. Lee and P. J. Rossky, *J. Chem. Phys.*, 1994, **100**, 3334–3345.
- 15 D. Laage and J. T. Hynes, *Science*, 2006, **311**, 832–835.
- 16 D. Laage and J. T. Hynes, *J. Phys. Chem. B*, 2008, **112**, 14230–14242.
- 17 D. Laage and J. T. Hynes, *Proc. Natl. Acad. Sci. U. S. A.*, 2007, **104**, 11167–11172.
- 18 F. Sterpone, G. Stirnemann, J. T. Hynes and D. Laage, *J. Phys. Chem. B*, 2010, **114**, 2083–2089.
- 19 G. Stirnemann, J. T. Hynes and D. Laage, *J. Phys. Chem. B*, 2010, **114**, 3052–3059.
- 20 J. Zheng, K. Kwak and M. D. Fayer, *Acc. Chem. Res.*, 2007, **40**, 75–83.
- 21 Y. S. Kim and R. M. Hochstrasser, *J. Phys. Chem. B*, 2009, **113**, 8231–8251.
- 22 J. J. Loparo, S. T. Roberts and A. Tokmakoff, *J. Chem. Phys.*, 2006, **125**, 194522.
- 23 H. J. C. Berendsen, J. R. Grigera and T. P. Straatsma, *J. Phys. Chem.*, 1987, **91**, 6269–6271.
- 24 J. C. Phillips, R. Braun, W. Wang, J. Gumbart, E. Tajkhorshid, E. Villa, C. Chipot, R. D. Skeel, K. Laxmikant and K. Schulten, *J. Comput. Chem.*, 2005, **26**, 1781–1802.
- 25 S. Mukamel, *Principles of Nonlinear Optical Spectroscopy*, Oxford University Press, New York, 1995.
- 26 J. B. Asbury, T. Steinel, C. Stromberg, S. A. Corcelli, C. P. Lawrence, J. L. Skinner and M. D. Fayer, *J. Phys. Chem. A*, 2004, **108**, 1107–1119.
- 27 J. R. Schmidt, S. A. Corcelli and J. L. Skinner, *J. Chem. Phys.*, 2005, **123**, 044513.
- 28 J. R. Schmidt, S. T. Roberts, J. J. Loparo, A. Tokmakoff, M. D. Fayer and J. L. Skinner, *Chem. Phys.*, 2007, **341**, 143–157.
- 29 The simulations used to calculate the spectra involved a smaller number of water molecules (500 instead of 1500) and infinite plates (obtained by adjusting the box size to the plate lattice parameters and periodic boundary conditions). The resulting distance between the

- two plates is 2.1 nm, and the water layer is approximately 1.2 nm thick. Although this confinement very slightly slows down the water dynamics, we verified that the vibrational spectra and their relaxation dynamics are not affected.
- 30 S. H. Northrup and J. T. Hynes, *J. Chem. Phys.*, 1980, **73**, 2700–2714.
- 31 M. Maccarini, *Biointerphases*, 2007, **2**, MR1–MR15.
- 32 K. R. Gallagher and K. A. Sharp, *J. Am. Chem. Soc.*, 2003, **125**, 9853–9860.
- 33 G. L. Richmond, *Chem. Rev.*, 2002, **102**, 2693–2724.
- 34 L. F. Scatena, M. G. Brown and G. L. Richmond, *Science*, 2001, **292**, 908–912.
- 35 P. N. Perera, K. R. Fega, C. Lawrence, E. J. Sundstrom, T.-P. J. and D. Ben-Amotz, *Proc. Natl. Acad. Sci. U. S. A.*, 2009, **106**, 12230–12234.
- 36 R. Ludwig, F. Weinhold and T. C. Farrar, *J. Chem. Phys.*, 1995, **103**, 6941–6950.
- 37 Y. L. A. Rezus and H. J. Bakker, *J. Chem. Phys.*, 2005, **123**, 114502.
- 38 S. Park, D. E. Moilanen and M. D. Fayer, *J. Phys. Chem. B*, 2008, **112**, 5279–5290.
- 39 D. Laage and J. T. Hynes, *Chem. Phys. Lett.*, 2006, **433**, 80–85.
- 40 J. Qvist and B. Halle, *J. Am. Chem. Soc.*, 2008, **130**, 10345–10353.
- 41 C. Mattea, J. Qvist and B. Halle, *Biophys. J.*, 2008, **95**, 2951–2963.
- 42 D. Laage, *J. Phys. Chem. B*, 2009, **113**, 2684–2687.
- 43 J. Teixeira, M.-C. Bellisent-Funel, S. H. Chen and A. J. Dianoux, *Phys. Rev. A: At., Mol., Opt. Phys.*, 1985, **31**, 1913–1917.
- 44 A. Luzar, *Faraday Discuss.*, 1996, **103**, 29–40.
- 45 It was recently shown<sup>42</sup> that interpretation of experimental neutron scattering results<sup>43</sup> with our jump model leads to reorientation times in agreement with those obtained through other techniques, while their original interpretation with the Debye rotational diffusion picture lead to times twice shorter.
- 46 Our jump reorientation mechanism contrasts with previous suggestions, such as ref. 44, as detailed in ref. 16.
- 47 A. R. Bizzarri and S. Cannistraro, *J. Phys. Chem. B*, 2002, **106**, 6617–6633.
- 48 S. L. Lee, P. G. Debenedetti and J. R. Errington, *J. Chem. Phys.*, 2005, **122**, 204511.
- 49 S. R. V. Castrillon, N. Giovambattista, I. A. Aksay and P. G. Debenedetti, *J. Phys. Chem. B*, 2009, **113**, 1438–1446.
- 50 M. G. Mazza, N. Giovambattista, F. W. Starr and H. E. Stanley, *Phys. Rev. Lett.*, 2006, **96**, 057803.
- 51 N. Agmon, E. Pines and D. Huppert, *J. Chem. Phys.*, 1988, **88**, 5631–5638.
- 52 S. H. Northrup and J. A. McCammon, *J. Chem. Phys.*, 1980, **72**, 4569–4578.
- 53 A. Luzar, *J. Chem. Phys.*, 2000, **113**, 10663–10675.
- 54 Approximating the back reaction from **B'** by a rate equation leads to a simple system of linear differential equations, in contrast to the explicit consideration of diffusion which requires a resolution through Laplace transforms.<sup>51,53</sup>
- 55 This was already observed and discussed in section IV.2. by examining the time dependent probability for an OH to form an angle  $\theta$  with respect to its initial orientation, as shown in Fig. 4a.
- 56 K. Seki, B. Bagchi and M. Tachiya, *Phys. Rev. E: Stat., Nonlinear, Soft Matter Phys.*, 2008, **77**, 031505.
- 57 A. Morita and J. T. Hynes, *J. Phys. Chem. B*, 2002, **106**, 673–685.
- 58 A. Morita and J. T. Hynes, *Chem. Phys.*, 2000, **258**, 371–390.
- 59 H. G. Hertz and M. D. Zeidler, *Ber. Bunsen-Ges. Phys. Chem.*, 1964, **68**, 821–837.
- 60 K. Matsuda, T. Hibi, H. Kadowaki, H. Kataura and Y. Maniwa, *Phys. Rev. B: Condens. Matter Mater. Phys.*, 2006, **74**, 073415.
- 61 A. W. Omta, M. F. Kropman, S. Woutersen and H. J. Bakker, *Science*, 2003, **301**, 347–349.
- 62 D. E. Moilanen, D. Wong, D. E. Rosenfeld, E. E. Fenn and M. D. Fayer, *Proc. Natl. Acad. Sci. U. S. A.*, 2009, **106**, 375–380.
- 63 A. Szabo, *J. Chem. Phys.*, 1984, **81**, 150–167.
- 64 H. J. Bakker, Y. L. A. Rezus and R. L. A. Timmer, *J. Phys. Chem. A*, 2008, **112**, 11523–11534.
- 65 J. D. Eaves, J. J. Loparo, C. J. Fecko, S. T. Roberts, A. Tokmakoff and P. L. Geissler, *Proc. Natl. Acad. Sci. U. S. A.*, 2005, **102**, 13019–13022.
- 66 J. J. Loparo, S. T. Roberts and A. Tokmakoff, *J. Chem. Phys.*, 2006, **125**, 194521.
- 67 M. L. Cowan, B. D. Bruner, N. Huse, J. R. Dwyer, B. Chugh, E. T. J. Nibbering, T. Elsaesser and R. J. D. Miller, *Nature*, 2005, **434**, 199–202.
- 68 S. Park, M. Odellius and K. J. Gaffney, *J. Phys. Chem. B*, 2009, **113**, 7825–7835.
- 69 A. Eftekhari-Bafrooei and E. Borguet, *J. Am. Chem. Soc.*, 2010, **132**, 3756–3761.
- 70 R. Rey, K. B. Moller and J. T. Hynes, *Chem. Rev.*, 2004, **104**, 1915–1928.
- 71 J. Bredenbeck, A. Ghosh, H.-K. Nienhuys and M. Bonn, *Acc. Chem. Res.*, 2009, **42**, 1332–1342.
- 72 J. Chowdhary and B. M. Ladanyi, *J. Phys. Chem. B*, 2009, **113**, 4045–4053.
- 73 J. Chowdhary and B. M. Ladanyi, *J. Phys. Chem. B*, 2008, **112**, 6259–6273.